Knight Shift and Leading Superconducting Instability from Spin Fluctuations in Sr_{2}RuO_{4}

A. T. Rømer, D. D. Scherer, I. M. Eremin, P. J. Hirschfeld, and B. M. Andersen

Phys. Rev. Lett. **123**, 247001 — Published 13 December 2019

DOI: 10.1103/PhysRevLett.123.247001

Knight Shift and Leading Superconducting Instability From Spin Fluctuations in Sr_2RuO_4

A. T. Rømer,[1,2] D. D. Scherer,[1] I. M. Eremin,[3] P. J. Hirschfeld,[4] B. M. Andersen[1]
[1] *Niels Bohr Institute, University of Copenhagen, Vibenhuset, Lyngbyvej 2, DK-2100 Copenhagen, Denmark*
[2] *Institut Laue-Langevin, 71 avenue des Martyrs CS 20156, 38042 Grenoble Cedex 9, France*
[3] *Institut für Theoretische Physik III, Ruhr-Universität Bochum, D-44801 Bochum, Germany*
[4] *Department of Physics, University of Florida, Gainesville, Florida 32611, USA*
(Dated: December 5, 2019)

Recent nuclear magnetic resonance studies [A. Pustogow *et al.*, arXiv:1904.00047] have challenged the prevalent chiral triplet pairing scenario proposed for Sr_2RuO_4. To provide guidance from microscopic theory as to which other pair states might be compatible with the new data, we perform a detailed theoretical study of spin-fluctuation mediated pairing for this compound. We map out the phase diagram as a function of spin-orbit coupling, interaction parameters, and band-structure properties over physically reasonable ranges, comparing when possible with photoemission and inelastic neutron scattering data information. We find that even-parity pseudospin singlet solutions dominate large regions of the phase diagram, but in certain regimes spin-orbit coupling favors a near-nodal odd-parity triplet superconducting state, which is either helical or chiral depending on the proximity of the γ band to the van Hove points. A surprising near-degeneracy of the nodal s'- and $d_{x^2-y^2}$-wave solutions leads to the possibility of a near-nodal time-reversal symmetry broken $s' + id_{x^2-y^2}$ pair state. Predictions for the temperature dependence of the Knight shift for fields in and out of plane are presented for all states.

Superconductivity in Sr_2RuO_4 remains largely a mystery despite the relative simplicity of the material as compared to the high-T_c cuprates and almost twenty five years of intense research efforts[1]. Until recently, the dominant opinion was that Sr_2RuO_4 represents a unique example of a chiral triplet superconducting state, supported by the presumed proximity of layered Sr_2RuO_4 to ferromagnetism[2], observed in the perovskite "parent" material $SrRuO_3$, as well as temperature independent Knight shift data across T_c, measured on both Ru[3, 4] and O[5, 6] nuclei. It was soon discovered, however, that the leading magnetic instability in Sr_2RuO_4 occurs in an antiferromagnetic, and not ferromagnetic channel[7–9], although later weak low q-fluctuations were also observed[10, 11]. In this case, the usual spin-fluctuation exchange pairing mechanism[12] would be expected to lead to even parity spin-singlet solutions rather than odd parity spin-triplet states. The situation is further complicated by the multi-orbital nature of the electronic states[7, 13], as well as sizeable spin-orbit coupling[14–18], resulting in significant magnetic anisotropy of the spin fluctuations in this material[10, 19, 20], which complicate theoretical analysis. Furthermore, as the main belief was that Sr_2RuO_4 supported a spin-triplet superconducting state, most theories focused on such solutions. For a review of earlier works see e.g. Ref. 1, and also more recent works, Refs.[21–26].

Very recently, the Knight shift in an in-plane magnetic field was re-measured by a different group and found to drop below T_c, severely challenging the prevalent chiral triplet pair state proposed for Sr_2RuO_4[27]. Previous results were interpreted as a result of heating of the sample during the application of high amplitude radio-frequency pulses [27]. This NMR result has been recently confirmed by another group[28], and therefore the problem of superconductivity in Sr_2RuO_4 is ripe for reexamination.

In this Letter we present a detailed theoretical study of spin-fluctuation mediated pairing relevant for Sr_2RuO_4 using a realistic spin-orbit coupling (SOC), which correctly reproduces the magnetic anisotropy found in this system, and sizeable Hund's coupling strength[29]. In particular, we investigate the leading superconducting instabilities in a framework where SOC is included both in the electronic structure and the pairing interaction. Throughout, we relate our results to neutron scattering data, and additionally discuss the Knight shift and the existence of nodal gaps in the DOS. Finally, we address the role of electron interactions beyond the random phase approximation (RPA) on the preferred Cooper pairing.

Atomic spin-orbit coupling, parametrized here by $H_{SOC} = \lambda_{soc}\mathbf{L}\cdot\mathbf{S}$, does not break time-reversal symmetry and due to Kramer's theorem all energies thus remain doubly degenerate. Degenerate eigenvectors are labelled by pseudo-spin $\sigma = +/-$ and the relation to electronic annihilation/creation operators $c_{\mu,s}(\mathbf{k})/c^\dagger_{\mu,s}(\mathbf{k})$ of orbital character μ and spin s is given by $\Psi(\mathbf{k},+) = [c_{xz\uparrow}(\mathbf{k}), c_{yz,\uparrow}(\mathbf{k}), c_{xy,\downarrow}(\mathbf{k})]$, and $\Psi(\mathbf{k},-) = [c_{xz,\downarrow}(\mathbf{k}), c_{yz,\downarrow}(\mathbf{k}), c_{xy,\uparrow}(\mathbf{k})]$. In this basis the non-interacting Hamiltonian can be written in block-diagonal form $\hat{H} = \sum_\sigma \Psi^\dagger(\mathbf{k},\sigma)(H_0 + H_{SOC})\Psi(\mathbf{k},\sigma)$ with the matrices H_0 and H_{SOC} given by

$$H_0 = \begin{pmatrix} \xi_{xz}(\mathbf{k}) & g(\mathbf{k}) & 0 \\ g(\mathbf{k}) & \xi_{yz}(\mathbf{k}) & 0 \\ 0 & 0 & \xi_{xy}(\mathbf{k}) \end{pmatrix}, \qquad (1)$$

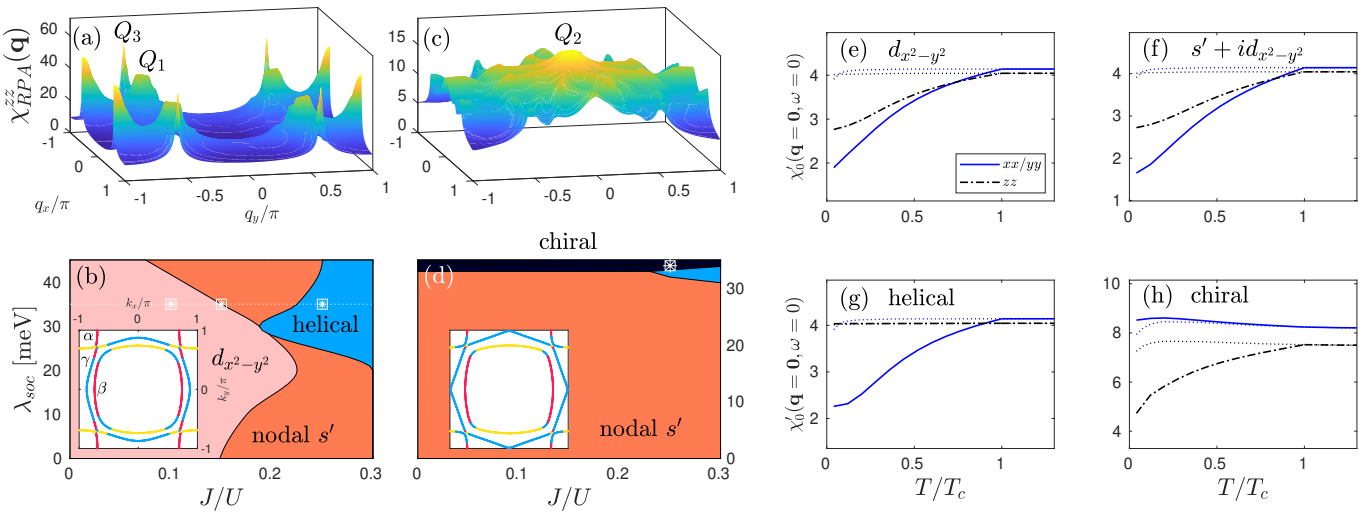

FIG. 1. Longitudinal spin susceptibility $\chi^{zz,\prime}_{RPA}(\mathbf{q},\omega=0)$ at $\lambda_{soc}=35$ meV and leading superconducting instability as a function of SOC amplitude λ_{soc} and Hund's coupling J for $\mu_{xy}=109$ meV (a,b) and $\mu_{xy}=134$ meV (c,d). The Fermi surface with the α,β and γ band is shown for each case by insets with dominating orbital content displayed by colors: xy-orbital is blue, xz is red and yz is yellow. In (b,d) white symbols display the positions for which the Knight shifts shown in (e-h) were obtained. The Knight shift is given by $\chi'_0(\mathbf{q}=0,\omega=0)$, and we set $k_BT_c=0.5$ meV and the maximum amplitude of the gap is $\Delta_{\max}=1$ meV. The solid blue line is the Knight shift for in-plane fields (xx/yy-component), while the black dashed-dotted line displays the Knight shift for out-of-plane fields (zz-component). The dotted lines display the normal state Knight shift xx/yy-component (blue) and zz-component (black).

$$H_{SOC}=\frac{1}{2}\begin{pmatrix}0 & -i\sigma\lambda_{soc} & i\lambda_{soc}\\ i\sigma\lambda_{soc} & 0 & -\sigma\lambda_{soc}\\ -i\lambda_{soc} & -\sigma\lambda_{soc} & 0\end{pmatrix}, \qquad (2)$$

with $\sigma=+(-)$ for pseudo-spin up (down) block. The electronic dispersions are given by $\xi_{xz}(\mathbf{k})=-2t_1\cos k_x-2t_2\cos k_y-\mu$, $\xi_{yz}(\mathbf{k})=-2t_2\cos k_x-2t_1\cos k_y-\mu$, and $\xi_{xy}(\mathbf{k})=-2t_3(\cos k_x+\cos k_y)-4t_4\cos k_x\cos k_y-2t_5(\cos 2k_x+\cos 2k_y)-\mu_{xy}$. As in Ref. 20 we parametrize the band by $\{t_1,t_2,t_3,t_4,t_5\}=\{88,9,80,40,5\}$ meV with $g(\mathbf{k})=0$ and the chemical potential of the xz,yz orbitals $\mu=109$ meV. Below, μ_{xy} is allowed to vary slightly from μ to map out the effect of a different crystal field, motivated by a sensitivity of the superconducting instability to the proximity of the xy orbital Fermi surface states to the van Hove saddle points. We restrict ourselves to a purely two-dimensional electronic model, given the strong electronic anisotropy of Sr_2RuO_4. Although the third dimension may play a role, the main physics is expected to occur in the RuO_2 planes.

We derive the effective electron-electron interaction in the Cooper channel from the multi-orbital Hubbard Hamiltonian which includes intra- and interorbital Coulomb interactions and Hund's coupling terms. Summation of all ladder and bubble diagrams gives the effective interaction expressed in terms of the bare interaction parameters U,U',J,J' and the RPA spin susceptibilities, for more details see Supplementary Material (SM) [30].

This procedure results in the interaction Hamiltonian

$$\hat{H}_{int}=\frac{1}{2}\sum_{\mathbf{k},\mathbf{k}'\{\tilde{\mu}\}}\Big[V(\mathbf{k},\mathbf{k}')\Big]^{\tilde{\mu}_1,\tilde{\mu}_2}_{\tilde{\mu}_3,\tilde{\mu}_4}c^\dagger_{\mathbf{k}\tilde{\mu}_1}c^\dagger_{-\mathbf{k}\tilde{\mu}_3}c_{-\mathbf{k}'\tilde{\mu}_2}c_{\mathbf{k}'\tilde{\mu}_4}, \qquad (3)$$

with the pairing interaction given by

$$\Big[V(\mathbf{k},\mathbf{k}')\Big]^{\tilde{\mu}_1,\tilde{\mu}_2}_{\tilde{\mu}_3,\tilde{\mu}_4}=\Big[U\Big]^{\tilde{\mu}_1,\tilde{\mu}_2}_{\tilde{\mu}_3,\tilde{\mu}_4}+\Big[U\frac{1}{1-\chi_0U}\chi_0U\Big]^{\tilde{\mu}_1\tilde{\mu}_2}_{\tilde{\mu}_3\tilde{\mu}_4}(\mathbf{k}+\mathbf{k}')-\Big[U\frac{1}{1-\chi_0U}\chi_0U\Big]^{\tilde{\mu}_1\tilde{\mu}_4}_{\tilde{\mu}_3\tilde{\mu}_2}(\mathbf{k}-\mathbf{k}'). \qquad (4)$$

The label $\tilde{\mu}=(\mu,s)$ is a joint index for orbital and electronic spin and $\chi_0=[\chi_0]^{\tilde{\mu}_1,\tilde{\mu}_2}_{\tilde{\mu}_3,\tilde{\mu}_4}(\mathbf{q},i\omega_n=0)$ denotes the real part of the static generalized multi-orbital spin susceptibility in the presence of SOC. The interaction Hamiltonian as stated in Eq. (3) is projected to band and pseudo-spin space to obtain the final form:

$$\hat{H}_{int}=\sum_{n,n',\mathbf{k},\mathbf{k}'}\sum_{l,l'}\overline{\Psi}_l(n,\mathbf{k})\,\frac{1}{2}\Gamma_{l,l'}(n,\mathbf{k};n',\mathbf{k}')\;\Psi_{l'}(n',\mathbf{k}'). \qquad (5)$$

Here n,n' are band indices, and the pseudo-spin information is carried by the l,l' indices with the fermion bilinear operator, $\Psi_l(n,\mathbf{k})$, defined in SM [30].

The leading and sub-leading superconducting instabilities are determined from the linearized gap equation

$$-\int_{FS}d\mathbf{k}'_f\,\frac{1}{v(\mathbf{k}'_f)}\Gamma_{l,l'}(\mathbf{k}_f,\mathbf{k}'_f)\Delta_{l'}(\mathbf{k}'_f)=\lambda\Delta_l(\mathbf{k}_f), \qquad (6)$$

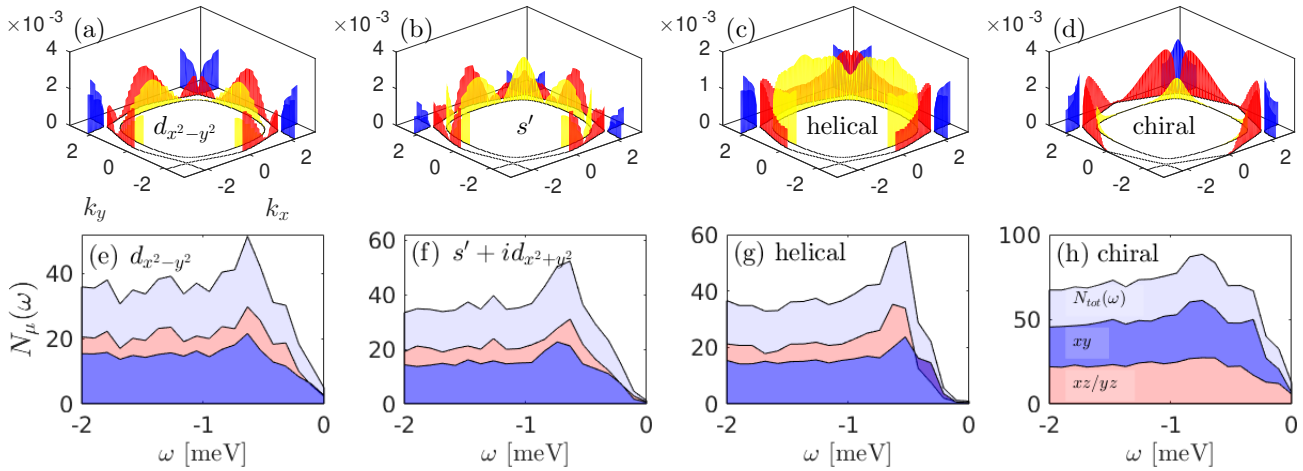

FIG. 2. Spectral gap $\Delta_{\mathbf{k}}$ for (a) $d_{x^2-y^2}$ ($J/U = 0.1$), (b) nodal s' ($J/U = 0.2$), (c) helical ($J/U = 0.25$) in the case of $\mu_{xy} = 109$ meV, $\lambda_{soc} = 35$ meV and $U = 120$ meV, see white stars in Fig. 1(b). (d) Spectral gap for the chiral solution with $\mu_{xy} = 134$ meV, $\lambda_{soc} = 35$ meV, $U = 50$ meV and $J/U = 0.25$. The band character of the gap is indicated by colors; α (blue), β (yellow) and γ (red). The band character generally corresponds directly to the orbital character, with the exception of the Fermi surface regions close to the zone diagonals as visualized in the Fermi surface insets in Fig. 1 (b,d). (e-h) Density of states for $\Delta_{\max} = 1$ meV. In panels (e,g,h) we invoke the gap structure in (a,c,d) while (f) shows $N_\mu(\omega)$ for a TRSB superconductor constructed by the complex superposition of the two even-parity solutions $d_{x^2-y^2}$ and s'.

where $\Delta_l(n,\mathbf{k}) = \frac{1}{2}\sum_{n',\mathbf{k}',l'}\Gamma_{l,l'}(n,\mathbf{k};n',\mathbf{k}')\langle\Psi_{l'}(n',\mathbf{k}')\rangle$. The integration in Eq. (6) includes momenta at the Fermi surface of the three bands with n uniquely defined by $\mathbf{k}_f$ and $v(\mathbf{k}_f)$ is the Fermi velocity at $\mathbf{k}_f$. The eigenvector $\Delta_l(\mathbf{k}_f)$ corresponding to the largest eigenvalue λ displays the structure of the leading superconducting instability.

The solutions to Eq. (6) are classified according to the tetragonal lattice symmetry restricted to two dimensions. The even parity states $\Delta_0(\mathbf{k})$ have four possible symmetries $\{s, d_{x^2-y^2}, d_{xy}, g\}$ while odd parity states fall either into one of the four possible superpositions of $\Delta_x(\mathbf{k})$ and $\Delta_y(\mathbf{k})$) (denoted helical states) or a chiral solution $\Delta_z(\mathbf{k})$, which is doubly degenerate. Here, $\{\Delta_x(\mathbf{k}), \Delta_y(\mathbf{k}), \Delta_z(\mathbf{k})\}$ denote the components of the vector $\mathbf{d}(\mathbf{k})$ [31] in the *pseudospin* space. The pseudospins are fixed in the plane perpendicular to the $\mathbf{d}$-vector. In our approach, the x and y components are degenerate, due to a lack of hybridization between the xz and yz orbitals. Therefore, all four helical states are degenerate, leaving open the possibility of complex superpositions of the type $\Delta_x + i\Delta_y$, which are non-unitary pair states breaking time-reversal symmetry (TRS).

In Fig. 1(a-d), we show the longitudinal (zz) component of the *spin* susceptibility and the leading superconducting instabilities as a function of SOC and Hund's coupling J for two different values of $\mu_{xy} = 109$, 134 meV, to expose the effect of van Hove proximity. The Fermi surface in each case is shown in the insets of Fig.1(b,d). The change in μ_{xy} has a strong effect on the physical susceptibilities, as shown in Fig. 1(a,c) where we plot $\chi^{zz}_{RPA}(\mathbf{q})$. For the band farthest from the van Hove point, we observe two prominent nesting vectors, which are approximately given by $\mathbf{Q}_1 = (2\pi/3, 2\pi/3)$ and $\mathbf{Q}_3 = (\pi, 2\pi/3)$, see Fig. 1(a). The vector $\mathbf{Q}_1$ arises from the nesting of the 1D-like xz/yz bands, see SM [30], and has been extensively reported by neutron scattering [8, 10, 32]. Furthermore, a factor two enhancement of the out-of-plane susceptibility compared to the in-plane susceptibility has been reported at this nesting vector [10]. Our calculations also give a spin anisotropy at $\mathbf{Q}_1$ with a magnitude that depends on both SOC, interaction parameters and the band structure, see SM [30]. As shown in Fig. 1, the regime where the spin susceptibility is dominated by $\mathbf{Q}_1$ and $\mathbf{Q}_3$ results in mainly even-parity solutions, which are both nodal, s' or $d_{x^2-y^2}$. A helical odd-parity pseudo-spin triplet solution is, however, favored in the regime of large SOC and Hund's coupling J, as seen in Fig. 1(b). We stress that for obtaining the results in Fig. 1, it is crucial to properly include SOC both in the band structure *and* in the pairing kernel, see SM [30]. Experimentally, the spin anisotropy observed by neutron scattering persist to 300 K [10] and photoemission fitting gives a value of $\lambda_{soc} = 32$ meV [17]. The Hund's coupling is estimated to be $J/U \simeq 0.1$ [33].

Only Fermi surfaces with a γ-band very close to the van Hove point produce a significant quasi-ferromagnetic signal $\mathbf{Q}_2$ originating mainly from intra-orbital xy nesting, see Fig. 1(c). At large values of λ_{soc}, chiral pseudo-spin triplet superconductivity emerges as shown in Fig. 1(d). However, when $\mathbf{Q}_2$ is less pronounced in better agreement with neutron experiments, the chiral state is entirely absent as a leading instability. For further parameter-dependence of the leading superconducting instability, we refer to the SM [30].

We note that a similar spin-fluctuation based approach was recently employed in Ref. 24, focusing on the very weak-coupling regime and small Hund's interaction. In this limit, chiral or helical solutions were found, whereas even-parity solutions dominated the regime of intermediate coupling strengths. One of our main findings, however, is that a helical state becomes again dominant for the larger values of the Hund's coupling and sizeable SOC, see Fig.1(b). In addition, the chiral state occurs only in regimes where the spin fluctuations appear inconsistent with available neutron scattering data.

The Knight shift provides a way to distinguish between even and odd-parity solutions found in Fig. 1(b,d). We address the Knight shift by a calculation of the uniform spin susceptibility in the superconducting state, $\chi_0'(\mathbf{q}=0,\omega=0)$ in four different gap scenarios; $d_{x^2-y^2}$, $s'+id_{x^2-y^2}$, helical and chiral superconductivity. The proposed solution $s'+id_{x^2-y^2}$ which displays time reversal symmetry breaking is restricted to the parameter space where s' and $d_{x^2-y^2}$ are degenerate.

If SOC was negligible, we would expect the Knight shift of the even-parity superconductors to be completely suppressed in all spin channels for $T\to 0$ [34] with exponential suppression for a full gap (s-wave) and linear suppression for a nodal gap. As seen in Fig. 1(e,f), the even-parity solutions do exhibit suppression in all spin channels, but more pronounced for the in-plane field directions, xx/yy. The simple expectation for singlet superconductors breaks down because a pseudo-spin singlet solution contains both electronic spin singlet *and* triplet character. To illustrate this point more clearly, we show in SM [30] how a conventional s-wave superconductor acquires a residual Knight shift at $T=0$ as an effect of SOC. The properties of helical and chiral solutions, however, remain largely as expected from the $\lambda_{soc}=0$ case: The helical superconductor exhibits a partial Knight shift suppression for in-plane fields and is insensitive to out-of-plane fields, see Fig. 1(g). For the chiral state shown in Fig. 1(h), the Knight shift is unaffected by in-plane fields and suppressed by out-of-plane magnetic fields, but full suppression is prevented by SOC [26].

Relating to the newest NMR results [27], our calculations reveal that the superconducting ground state in Sr_2RuO_4 is consistent either with an even-parity pseudo-spin singlet or a helical pseudo-spin triplet pair state. Future NMR measurements for out-of-plane fields should be able to distinguish between these cases: the helical solution should exhibit no suppression, while the even-parity solution should display a clear suppression. Finally, we note that a possible non-unitary TRSB state of the type $\Delta_x+i\Delta_y$ would display the same Knight shift as the helical solution.

Turning to the spectral properties of the various superconducting states found above, an outstanding experimental puzzle is the experimental observation of nodes (or near-nodes) in the density of states (DOS) [35–40].

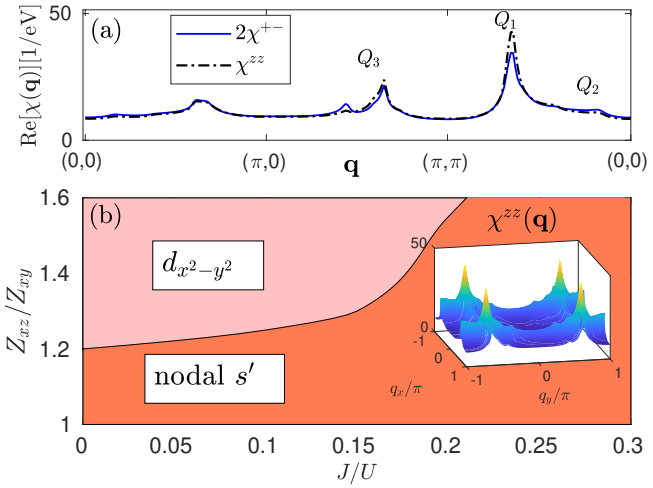

FIG. 3. (a) $\chi^{zz}(\mathbf{q})/\chi^{+-}(\mathbf{q})$ along the path $(0,0)-(\pi,0)-(\pi,\pi)-(0,0)$ in the case of $Z_{xz}/Z_{xy}=1.6$ for a band with $\mu=$ 90 meV, $\mu_{xy}=128$ meV and $\lambda_{soc}=35$ meV. The signal at $\mathbf{Q}_1$ dominates and exhibits a spin anisotropy in rough agreement with experiments [10].(b) Leading superconducting instability for μ,μ_{xy} and λ_{soc} as in (a) as a function of quasi-particle weight anisotropy Z_{xz}/Z_{xy} and J. The inset shows $\chi^{zz}(\mathbf{q})$.

For the details of the DOS calculations we refer to the SM section [30]. The $d_{x^2-y^2}$ solution found in Fig. 1(b) has symmetry-imposed line nodes, with a gap that rises very steeply away from the zone diagonals, as shown in Fig. 2 (a). The nodes give rise to the characteristic V-shaped DOS at the Fermi level, as shown in Fig. 2(e). The s' solution, which appears to be very prominent in a large region of phase space also exhibits nodes, see Fig. 2(b), but in general the nodes do not coincide with the nodes of $d_{x^2-y^2}$-wave. However, the β-pocket shows a suppressed $d_{x^2-y^2}$ gap in the region where the s' solution has nodes. Therefore, the TRSB solution of the type $s'+id_{x^2-y^2}$ will exhibit near-nodal behavior with a small DOS close to the Fermi level, as seen in Fig. 2 (f). The helical state gives rise to a more uniform spectral gap, see Fig. 2(c), with near-nodal behavior only at the α pockets at the zone diagonals. Thus, in this case, we find a more complete suppression of the DOS at the smallest energies, see Fig. 2(g). Finally, for the chiral solution, only segments of the Fermi surface which are predominantly of xy orbital character, display a large gap, as can be deduced by comparing the spectral gap of Fig. 2(d) with the orbital character of the Fermi surface displayed in the inset of Fig. 1(d). Parts of the Fermi surface which are of xz/yz character exhibit almost no gap, and thus there remains a large number of electronic states close to the Fermi surface as evident from Fig. 2 (h). We note that this appears to agree with the findings of the recent work by Wang *et al.* [26], where a chiral solution was found to have low-lying states. The chiral state, however, appears to be ruled out by the recent NMR results [27].

In Sr_2RuO_4 significant mass renormalizations have

been identified from DMFT originating from the proximity of the van Hove singularity [41] and Hund's coupling, driving the effective mass of the xy orbital larger than the effective mass of xz/yz orbitals. To investigate how this changes the gap solutions, we apply the same approach as in Refs. [42, 43]. Thus, the bare electronic operator is modified by $c_{\mathbf{k},\mu,s} \rightarrow \sqrt{Z_\mu} c_{\mathbf{k},\mu,s}$ and a difference in quasi-particle weights between the xy orbital and the xz/yz orbitals is imposed by $Z_{xz} = Z_{yz} > Z_{xy}$. The quasi-particle weights dress the susceptibility[42]

$$[\tilde{\chi}_0]^{\tilde{\mu}_1,\tilde{\mu}_2}_{\tilde{\mu}_3,\tilde{\mu}_4} \rightarrow \sqrt{Z_{\mu_1}}\sqrt{Z_{\mu_2}}\sqrt{Z_{\mu_3}}\sqrt{Z_{\mu_4}}\,[\chi_0]^{\tilde{\mu}_1,\tilde{\mu}_2}_{\tilde{\mu}_3,\tilde{\mu}_4}\,, \qquad (7)$$

and the interaction Hamiltonian Eq. (3). In Fig. 3(a) we show how the orbital-selective quasi-particle weights lead to improved agreement with the spin susceptibility as measured be neutron scattering[8–10, 32]. For example, the signal at $\mathbf{Q}_3$ in Fig. 1(a) which originates from interband nesting between the xy orbital and the xz/yz bands has been reported by neutron scattering only in Ref.[32], interpreted as a ridge of the $\mathbf{Q}_1$ peak with weaker intensity.

A suppression of the response at $\mathbf{Q}_3$ as well as $\mathbf{Q}_2$ is observed when we calculate the spin response in the case of stronger mass enhancement of the xy orbital compared to the xz/yz orbitals [41] ($Z_{xz}/Z_{xy} > 1$). This scenario leaves the spin anisotropic response at $\mathbf{Q}_1$ the main magnetic feature of our calculation and provides a route to closer agreement with neutron scattering observations. In this approach, the linearized gap equation results in either nodal s' or $d_{x^2-y^2}$ solutions, and a notable absence of odd-parity pair states, as shown in the phase diagram Fig. 3 (b). The large boundary between the two solutions points to the possibility of a $s' + id_{x^2-y^2}$ gap structure which could reconcile the properties of 1) a decrease in Knight shift for in-plane fields at $T < T_c$, 2) nodal low-energy electronic states available for transport, and 3) signatures of TRSB [44, 45][46].

In summary we have provided a timely theoretical study of the leading superconducting instabilities in Sr_2RuO_4. We have discussed their spectral and magnetic properties and focused on recent neutron scattering and Knight shift measurements, which seem inconsistent with chiral triplet pairing and point to other preferred pair states for this material. Several possibilities are discussed, including a rare helical triplet state and more prevalent even-parity pair states which, as we have shown, can be distinguished by future experiments.

The authors are grateful for illuminating discussions with S. Brown, P. Kotetes, A. Kreisel, S. Mukherjee, S. Raghu and P. Steffens. A.T.R., D.D.S., and B.M.A. acknowledge support from the Carlsberg Foundation. P.J.H. was supported by the U.S. Dept. of Energy under Grant No. DE-FG02- 05ER46236.

[1] A. P. Mackenzie, T. Scaffidi, C. W. Hicks, and Y. Maeno, npj Quantum Materials **2**, 40 (2017).
[2] M. Sigrist, D. Agterberg, A. Furusaki, C. Honerkamp, K. Ng, T. M. Rice, and M. E. Zhitomirsky, Physica C **317-318**, 134 (1999).
[3] K. Ishida, Y. Kitaoka, K. Asayama, S. Ikeda, S. Nishizaki, Y. Maeno, K. Yoshida, and T. Fujita, Phys. Rev. B **56**, R505(R) (1997).
[4] K. Ishida, M. Manago, T. Yamanaka, H. Fukazawa, Z. Q. Mao, Y. Maeno, and K. Miyake, Phys. Rev. B **92**, 100502(R) (2015).
[5] M. H. K. Y. A. K. M. Z. Q. M. Y. Ishida, K. and Y. Maeno, Nature **396**, 658 (1998).
[6] M. Manago, K. Ishida, Z. Mao, and Y. Maeno, Phys. Rev. B **94**, 180507(R) (2016).
[7] I. I. Mazin and D. J. Singh, Phys. Rev. Lett. **82**, 4324 (1999).
[8] Y. Sidis, M. Braden, P. Bourges, B. Hennion, S. NishiZaki, Y. Maeno, and Y. Mori, Phys. Rev. Lett. **83**, 3320 (1999).
[9] M. Braden, Y. Sidis, P. Bourges, P. Pfeuty, J. Kulda, Z. Mao, and Y. Maeno, Phys. Rev. B **66**, 064522 (2002).
[10] M. Braden, P. Steffens, Y. Sidis, J. Kulda, P. Bourges, S. Hayden, N. Kikugawa, and Y. Maeno, Phys. Rev. Lett. **92**, 097402 (2004).
[11] P. Steffens, Y. Sidis, J. Kulda, Z. Q. Mao, Y. Maeno, I. I. Mazin, and M. Braden, Phys. Rev. Lett. **122**, 047004 (2019).
[12] N. Berk and J. Schrieffer, Phys. Rev. Lett. **17**, 433 (1966).
[13] T. Oguchi, Phys. Rev. B **51**, 1385 (1995).
[14] K. Ng and M. Sigrist, EPL **49**, 473 (2000).
[15] J. F. Annett, G. Litak, B. L. Györffy, and K. I. Wysokinski, Phys. Rev. B **73**, 134501 (2006).
[16] M. W. Haverkort, I. S. Elfimov, L. H. Tjeng, G. A. Sawatzky, and A. Damascelli, Phys. Rev. Lett. **101**, 026406 (2008).
[17] V. Zabolotnyy, D. Evtushinsky, A. Kordyuk, T. Kim, E. Carleschi, B. Doyle, R. Fittipaldi, M. Cuoco, A. Vecchione, and S. Borisenko, Journal of Electron Spectroscopy and Related Phenomena **191**, 48 (2013).
[18] C. N. Veenstra, Z.-H. Zhu, M. Raichle, B. M. Ludbrook, A. Nicolaou, B. Slomski, G. Landolt, S. Kittaka, Y. Maeno, J. H. Dil, I. S. Elfimov, M. W. Haverkort, and A. Damascelli, Phys. Rev. Lett. **112**, 127002 (2014).
[19] I. Eremin, D. Manske, and K.-H. Bennemann, Phys. Rev. B **65**, 220502(R) (2002).
[20] S. Cobo, F. Ahn, I. Eremin, and A. Akbari, Phys. Rev. B **94**, 224507 (2016).
[21] S. Raghu, S. A. Kivelson, and D. J. Scalapino, Phys. Rev. B **81**, 224505 (2010).
[22] Q. Wang, C. Platt, Y. Yang, C. Honerkamp, F. Zhang, W. Hanke, T. Rice, and R. Thomale, EPL **104**, 17013 (2013).
[23] T. Scaffidi, J. C. Romers, and S. H. Simon, Phys. Rev. B **89**, 220510(R) (2014).
[24] L.-D. Zhang, W. Huang, F. Yang, and H. Yao, Phys. Rev. B **97**, 060510(R) (2018).
[25] O. Gingras, R. Nourafkan, A.-M. S. Tremblay, and M. Côté, pre-print (2018), arXiv:1808.02527.
[26] W.-S. Wang, C.-C. Zhang, F.-C. Zhang, and Q.-H. Wang, Phys. Rev. Lett. **122**, 027002 (2019).

[27] A. Pustogow, Y. Luo, A. Chronister, Y. S. Su, D. A. Sokolov, F. Jerzembeck, A. Mackenzie, C. W. Hicks, N. Kikugawa, S. Raghu, E. D. Bauer, and S. E. Brown, pre-print (2019), arXiv:1904.00047.

[28] K. Ishida, "Nmr and nqr studies on sr2ruo4," Invited talk at the conference: Strontium Ruthenate, 25 years of a puzzling superconductor, Zurich, May 9-11 (2019).

[29] M. Kim, J. Mravlje, M. Ferrero, O. Parcollet, and A. Georges, Phys. Rev. Lett. **120**, 126401 (2018).

[30] See Supplemental Material [url] which includes Ref. [47], providing additional details about the spin susceptibility, the leading and sub-leading instabilities of the superconducting order and the sensitivity to the electronic bands, spin-orbit coupling and interaction strengths. In addition, a derivation the effective pairing interaction in the presence of spin-orbit coupling is presented and details of the linearized gap equation, the Knight shift and the density of states calculations are included.

[31] M. Sigrist and K. Ueda, Rev. Mod. Phys. **63**, 239 (1991).

[32] K. Iida, M. Kofu, N. Katayama, J. Lee, R. Kajimoto, Y. Inamura, M. Nakamura, M. Arai, Y. Yoshida, M. Fujita, K. Yamada, and S.-H. Lee, Phys. Rev. B **84**, 060402(R) (2011).

[33] L. Vaugier, H. Jiang, and S. Biermann, Phys. Rev. B **86**, 165105 (2012).

[34] K. Yosida, Phys. Rev. **110**, 769 (1958).

[35] E. Hassinger, P. Bourgeois-Hope, H. Taniguchi, S. René de Cotret, G. Grissonnanche, M. S. Anwar, Y. Maeno, N. Doiron-Leyraud, and L. Taillefer, Phys. Rev. X **7**, 011032 (2017).

[36] M. Suzuki, M. A. Tanatar, N. Kikugawa, Z. Q. Mao, Y. Maeno, and T. Ishiguro, Phys. Rev. Lett. **88**, 227004 (2002).

[37] K. Ishida, H. Mukuda, Y. Kitaoka, Z. Q. Mao, Y. Mori, and Y. Maeno, Phys. Rev. Lett. **84**, 5387 (2000).

[38] I. Bonalde, B. D. Yanoff, M. B. Salamon, D. J. Van Harlingen, E. M. E. Chia, Z. Q. Mao, and Y. Maeno, Phys. Rev. Lett. **85**, 4775 (2000).

[39] K. Deguchi, Z. Q. Mao, H. Yaguchi, and Y. Maeno, Phys. Rev. Lett. **92**, 047002 (2004).

[40] H. Suderow, J. P. Brison, J. Flouquet, A. W. Tyler, and Y. Maeno, Journal of Physics: Condensed Matter **10**, L597 (1998).

[41] J. Mravlje, M. Aichhorn, T. Miyake, K. Haule, G. Kotliar, and A. Georges, Phys. Rev. Lett. **106**, 096401 (2011).

[42] A. Kreisel, B. M. Andersen, P. O. Sprau, A. Kostin, J. C. S. Davis, and P. J. Hirschfeld, Phys. Rev. B **95**, 174504 (2017).

[43] P. O. Sprau, A. Kostin, A. Kreisel, A. E. Böhmer, V. Taufour, P. C. Canfield, S. Mukherjee, P. J. Hirschfeld, B. M. Andersen, and J. C. S. Davis, Science **357**, 75 (2017), https://science.sciencemag.org/content/357/6346/75.full.pdf.

[44] G. M. Luke, Y. Fudamoto, K. M. Kojima, M. I. Larkin, J. Merrin, B. Nachumi, Y. J. Uemura, Y. Maeno, Z. Q. Mao, Y. Mori, H. Nakamura, and M. Sigrist, Nature **394**, 558 (1998).

[45] A. Kapitulnik, J. Xia, E. Schemm, and A. Palevski, New Journal of Physics **11**, 055060 (2009).

[46] We note that our 2D calculations are not capable of capturing pairing instabilities that pair electrons between two layers, as proposed in Ref. 27.

[47] A. T. Rømer, A. Kreisel, I. Eremin, M. A. Malakhov, T. A. Maier, P. J. Hirschfeld, and B. M. Andersen, Phys. Rev. B **92**, 104505 (2015).